XVI International Conference on Durability of Building Materials and Components
DBMC 2023, China
K.F. Li and D.P. Fang (Eds)

Experimental Study of the Development of Stresses in Prestressing Strands under Different Environments

Dandan Xu [1], Chen Chen[1] and Yuxi Zhao [1*]

[1]College of Civil Engineering And Architecture, Zhejiang University, Hangzhou 310058, PR China, xuddan@zju.edu.cn (Dandan Xu), 22012034@zju.edu.cn (Chen Chen), yuxizhao@zju.edu.cn (Yuxi Zhao)

Abstract. *This paper presents findings from an experimental study on the effects of different environmental factors on post-tensioned prestressed concrete beams. The study included four different environments: outdoor shielded, drying-wetting cycles with tap water, drying-wetting cycles with NaCl solution, and drying-wetting cycles with NaCl solution and energized longitudinal rebars. A vibrating-string anchor cable dynamometer was used to measure the stress variation in prestressing strands. The results indicate that ambient temperature affects the trend of stresses in the prestressing strands. The increasing humidity caused by drying-wetting cycles and increasing salinity caused by NaCl solution led to the expansion of the concrete and increased stresses in the prestressing strands. Additionally, the corrosion of longitudinal rebars caused by the impressed-current accelerated corrosion method results in concrete damage and cracking, and continuously decreases the stresses in the prestressing strands. The study is ongoing, and further observations and reports will be made to evaluate the effects of different environmental factors on stresses in prestressing strands of post-tensioned beams.*

Keywords: *Steel Corrosion, Prestressed Concrete Beam, Drying-wetting Cycles, Prestress Loss.*

1 Introduction

Prestressed concrete (PC) structures are widely utilized worldwide due to their favorable mechanical properties. However, the invasion of corrosive agents in the service environment has caused numerous durability problems induced by steel corrosion within prestressed concrete structures. These issues have led to failures of engineering structures in recent years (Powers et al. 2002, Menga et al. 2022). The influence of steel corrosion on prestressed concrete structures is often reflected in the prestress loss, which degrades over time and significantly affects their long-term deflection and service behavior, even jeopardizing the structures' safety.

Despite the significance of steel corrosion on prestress loss, few studies focus on its mechanism and effect on prestress loss (Dasar et al. 2016, Dai et al. 2020, Li et al. 2022). Moreover, the majority of related research has concentrated on the corrosion of prestressing tendons, with limited attention given to the corrosion of nonprestressed reinforcement. However, nonprestressed reinforcements are closer to the surface of the prestressed concrete members, making them more susceptible to corrosion, and their presence affects prestress loss (Kottari & Shing 2014, Youakim et al. 2007). Therefore, it is necessary to study the effect of nonprestressed reinforcement corrosion on prestress loss.

Furthermore, prior experimental studies have overlooked the effects of humidity changes caused by drying-wetting cycles and salinity changes caused by sodium chloride solution on concrete that can affect prestress loss, despite always employing the drying-wetting cycles and the impressed-current accelerated corrosion method.

This study aims to investigate the stress variation in prestressing strands of prestressed beams under different environments by experimental observations. To achieve this goal, four beams in four different environments are studied. During the 180-day experimental observation period, the prestressing force in the prestressing strands is measured using a vibrating-string anchor cable dynamometer. The study compares the stress variation of the beams in different environments and focuses on the effect of environmental factors including humidity and salinity introduced by the accelerated corrosion method and corrosion of longitudinal rebars on the stress in prestressing strands.

2 Experimental Program

2.1 Specimens Design and Fabrication

The experimental program involved testing four post-tensioned prestressed concrete beams, all with identical geometry, featuring a cross-sectional size of 200×200 mm and a total length of 1600 mm. Figure 1 provides detailed information about the beam dimensions and cross-sectional details.

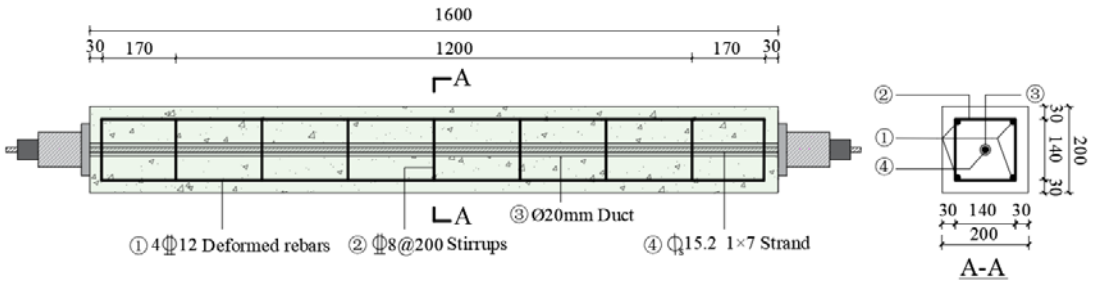

Figure 1. Beam dimensions and cross-section details (dimensions in mm).

Prestressing is provided by a 15.2 mm diameter seven-wire strand, placed at the center of the section and protected by a corrugated plastic pipe without grouting embedded in the concrete. The nonprestressed rebars consisted of two types of HRB400 ribbed bars: 8 mm diameter stirrups with epoxy coated against corrosion, and four longitudinal rebars of 12 mm diameter. The mechanical properties of prestressing strands and rebars are given in Table 1.

Table 1. Mechanical properties of prestressing strands and rebars (MPa).

Type of reinforcement	Yield strength	Ultimate strength	Modulus of elasticity
Ordinary rebars	435	606	2.05×10^5
Prestressing strands	-	1908	1.96×10^5

The mixture proportion of concrete used in this test is provided in Table 2. Cubic concrete blocks in 150×150×150 mm and prism concrete blocks in 150×150×300 mm were cast using the same concrete and cured under the same condition as that in the beams. The 28-day compressive strength and modulus of elasticity of concrete were determined from the cubic concrete blocks and prism concrete blocks, as shown in Table 3. After 28 days of curing, each

prestressing strand was post-tensioned up to 70% of its nominal ultimate tensile strength using an electric tensioning oil pump and hydraulic jack.

Table 2. Mix proportion of concrete (kg/m3).

Materials	Cement	Fly ash	lag	Fine aggregate	Coarse aggregate	Water	Water reducing agent
Quantities	370	50	50	840	1010	185	2

Table 3. Mechanical properties of concrete at 28 days (MPa).

Cubic compressive strength	Prism compressive strength	Modulus of elasticity
44.21	28.90	3.1×10^4

2.2 Accelerated Corrosion Process

After post-tensioning, the four test beams were positioned in a sheltered atmospheric outdoor environment for a period of 120 days. Following this, each beam was exposed to distinct test environments, as detailed in Table 4. Beam N was utilized as a control.

Table 4. Exposed environments of beams.

Beam notation	Test environment
N	sheltered atmospheric outdoor environment
DW-H_2O-L	drying-wetting cycles with tap water
DW-NaCl-L	drying-wetting cycles with 5%NaCl solution
DW-NaCl-LQ	drying-wetting cycles with 5%NaCl solution and energized longitudinal rebars

In the case of drying-wetting cycles, every cycle spanned 7 days, including a 3-day wetting period followed by a 4-day drying period. During the wetting period, the beam was covered with a sponge immersed in tap water or 5% NaCl solution and subsequently wrapped in plastic film to mitigate water evaporation, as illustrated in Figure 2(a). During the drying period, the damp sponge was removed, and the beams were directly exposed to the atmosphere. In the impressed-current accelerated method, a sponge immersed in 5% NaCl solution was used to cover the beam and then a stainless-steel net was positioned on the sponge. The longitudinal rebar served as an anode while the stainless-steel net acted as a cathode. An impressed current with a density of 60 $\mu A/cm^2$ was applied to hasten the corrosion process, as depicted in Figure 2(b). For beam DW-NaCl-LQ, the drying-wetting cycles and the impressed-current accelerated method were synchronized. Power was activated during the wetting period and disconnected during the drying period. The study focused only on the corrosion of longitudinal rebars, and the stirrups were shielded from corrosion by epoxy resin coating.

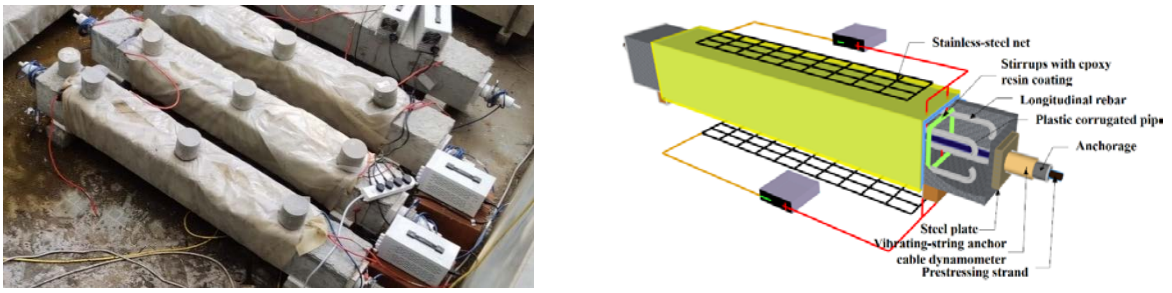

Figure 2. (a) Beams with the damp sponge and plastic film wrapping (in the wetting period); **(b)**The impressed-current accelerated corrosion test set-up.

2.3 Measurement of Stresses in Prestressing Strands

The vibrating-string anchor cable dynamometer was utilized in this study to measure the stress variation in prestressed strands, and it was installed between the concrete beam's end and the anchorage. The dynamometer features several vibrating chord strain gauges inside the steel cylinder, allowing it to detect compression forces. The compression force is calculated by substituting the calibration coefficient (Lai 2016) into Equation (1):

$$F = k(f_i^2 - f_0^2) \tag{1}$$

Where k is the characteristic coefficient of the dynamometer (kN/Hz^2), and the value is taken from the instrument manual; f_0 and f_i are the dynamometer's initial frequency and measurement frequency (Hz), respectively.

The stress in prestressing strands can be obtained by dividing the value of compression force by the cross-sectional area of prestressing strands. The stress variation in prestressing strands $\Delta\sigma(t)$ at t days can be obtained by Equation (2):

$$\Delta\sigma(t) = \sigma(t) - \sigma(0) \tag{2}$$

Where $\sigma(0)$ is the stress in prestressing strands before the test (120d after jacking) (N/mm^2); $\sigma(t)$ is the stress in prestressing strands at t days in the test environment (N/mm^2). A positive value of $\Delta\sigma(t)$ indicates an increase in the stress of prestressing strands in the test environment, whereas a negative value indicates a decrease.

3 Results and Discussion

3.1 Variation of Stresses in Prestressing Strands

The time-dependent values of stress variation in prestressing strands of beams were monitored using the vibrating-string anchor cable dynamometer as illustrated in Figure 3(a). The control beam N exhibited an initial decline phase, unlike the other test beams, which is probably due to the ongoing shrinkage and creep of concrete, leading to the prestress loss and a decrease in the stress in the prestressing strands.

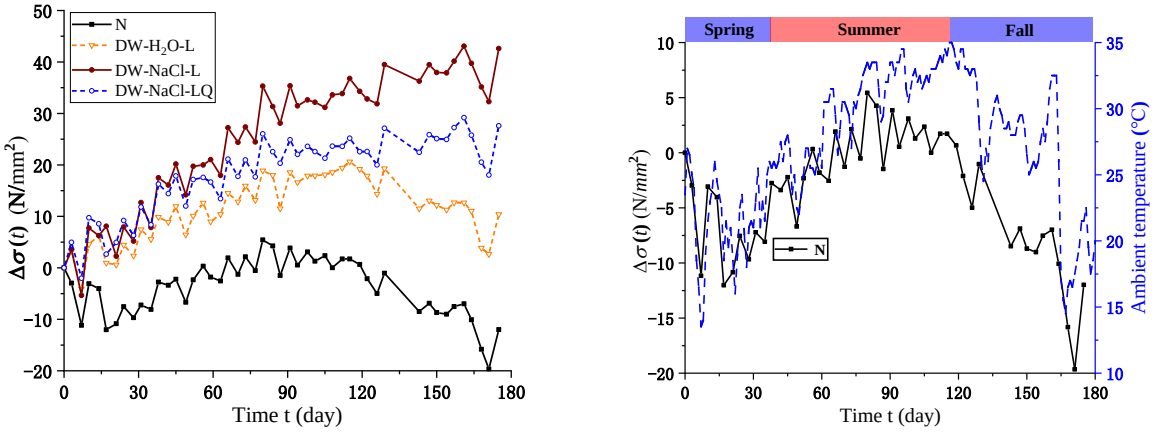

Figure 3. (a) The stress variation in prestressing strands (120d after jacking); **(b)**The stress variation in the prestressing strand of beam N and ambient temperature during the monitoring period.

Subsequently, the control beam N showed an overall trend of increasing and then decreasing, which may be attributed to the change in ambient temperature. As shown in Figure 3(b), the variation of stress in the prestressing strand of beam N exhibited fluctuations during the whole measurement period, and the trend of fluctuations was generally consistent with that of the ambient temperature. This may be attributed to the temperature deformation of concrete or the initial frequency drift caused by the thermal expansion of the sensor in the dynamometer due to the ambient temperature. As a result, an increase in the stress of prestressing strands was measured at higher temperatures (and vice versa).

The effect of ambient temperature is also evident in the other test beams, and it can be observed that the curve shapes of the test beams and beam N are very similar, except for the initial declining phase of beam N. This section focuses on the reasons for the stress variation in the prestressing strand of beam N, while the discussion of the changing tendency for the other three test beams is detailed in sections 3.2~3.4.

3.2 Effects of Humidity

The difference curve of Δσ(t) was obtained by subtracting the stress variation values Δσ(t) in the prestressing strand of beam N from that of beam DW-H_2O-L, as shown in Figure 4. This calculation eliminates the impact of ambient temperature and highlights the impact of humidity on the stress in the prestressing strand. Figure 4 demonstrates that the stress in the prestressing strand shows a positive correlation with time. However, the growth rate of the stress reduces gradually, leading to a state of stabilization.

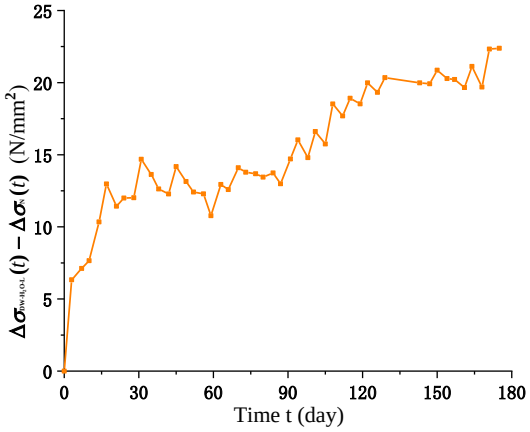

Figure 4. The difference curve of Δσ(t) of beam DW-H_2O-L and beam N.

This behavior is associated with humidity changes introduced by drying-wetting cycles. During the initial stages of the drying-wetting cycles, the concrete absorbs water and expands, thus recovering the compression deformation caused by the initial prestressing. This expansion increases the distance between the anchorages at both ends of the beam, elongating the prestressing strand and increasing the stress in the prestressing strand. However, this trend eventually stabilizes as the concrete absorbs sufficient water.

3.3 Effects of Salinity

The difference curve of Δσ(t) was derived by subtracting the stress variation values Δσ(t) in the prestressing strand of beam DW-H_2O-L from that of beam DW-NaCl-L, as shown in Figure 5. This calculation eliminates the interference of ambient temperature and drying-wetting cycles, providing a clear reflection of the effect of salinity on the stress in the prestressing strand.

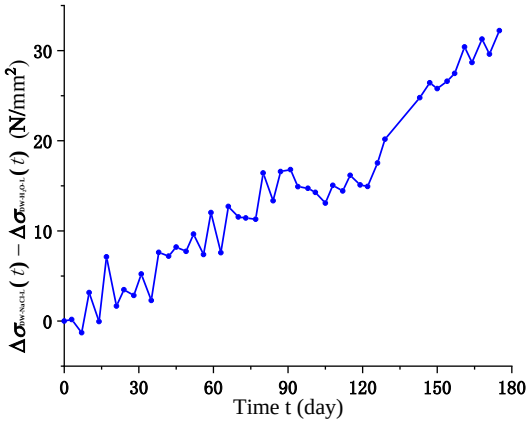

Figure 5. The difference curve of Δσ(t) of beam DW-NaCl-L and beam DW-H_2O-L.

Figure 5 indicates a continuous increase in stress in the prestressing strand over time, attributed to the crystallization of chloride salts in the concrete pores, resulting in expansion. Within concrete, a multitude of through capillaries exists. During drying-wetting cycles with 5% NaCl solution, the solution infiltrates the concrete through capillary action during the

wetting period. Water evaporation during the subsequent drying period results in an increase in the solution concentration, ultimately surpassing its solubility concentration, leading to the crystallization of chloride salts in the concrete pores (Ma 2009). This process causes the volume of the concrete to expand, leading to an increase in the distance between the anchorages at both ends of the beam. The anchorage clips prevent relative slip between the anchorage and the prestressing strand, ultimately causing the prestressing strand to elongate, thus increasing the stress in the prestressing strand. During this study period, the concentration of chloride salt solution within the concrete increased over time, resulting in the increase of salt crystallization pressure, and thus the corresponding stress in the prestressing strand continued to grow.

3.4 Effects of Corrosion of Longitudinal Rebars

Through a comparison of the stress variation Δσ(t) in the prestressing strand of beam DW-NaCl-LQ and beam DW-NaCl-L in Figure 3(b), any interference from ambient temperature, salinity, and humidity was eliminated to obtain the effects of corrosion of the longitudinal rebars. The results are depicted in Figure 6, which shows the difference curve obtained by subtracting the stress variation in beam DW-NaCl-L from that in beam DW-NaCl-LQ.

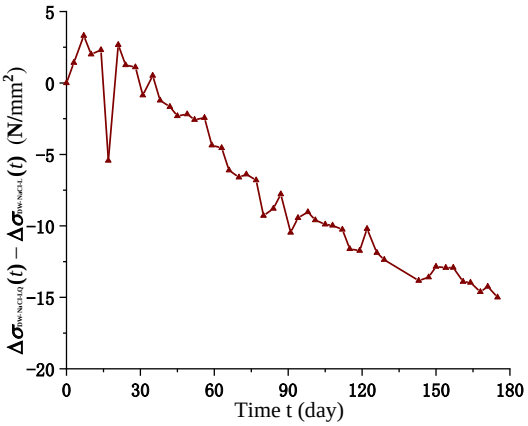

Figure 6. The difference curve of Δσ(t) of beam DW-NaCl-LQ and beam DW-NaCl-L.

From this figure, it is clear that the continual decrease in stress of the prestressing strand and a negative correlation with time. This decrease is due to the rapid corrosion of the longitudinal rebars under impressed-current accelerated corrosion, which leads to longitudinal cracking of the concrete, damage to concrete materials, degradation of concrete stiffness, and an increase in concrete deformation. Consequently, the distance between the anchorages at both ends of the beam decreases, causing a decrease in the stress in the prestressing strand. Furthermore, the creep of concrete increases after concrete cracking, which results in an increase in prestress loss and a subsequent decrease in stress in the prestressing strand. The continuous decrease of the curve in Figure 6 indicates an increase in corrosion-induced cracking damage of concrete due to impressed current, resulting in a decrease in the stress of the prestressing strand.

4 Conclusions

- The stress trends in prestressing strands were found to be consistent with the ambient temperature, which could be attributed to temperature deformation of concrete or the

temperature drift of the dynamometer sensor's initial frequency.

- The humidity caused the stresses in prestressing strands to increase gradually with time but eventually stabilized because concrete no longer expands when saturated.
- The salinity caused a continuous increase in stress in prestressing strands due to the expansion of concrete caused by salt crystallization and its associated pressure.
- The corrosion of longitudinal rebars caused by the impressed-current accelerated corrosion method resulted in concrete damage and cracking, leading to a continuous decrease in stress in prestressing strands.

This experimental study is ongoing, and the effects of environmental factors on the stresses in the prestressing strands in post-tensioned beams will be continuously observed and reported.

Acknowledgments

Financial support from Key Technology of High-Performance Prestressed Engineering Structure System and Application (2022YFC3801801), the National Key R&D Program of China, and the National Natural Science Foundation of China (52038010) are gratefully acknowledged.

References

Dai, L., Bian, H., Wang, L., Potier-Ferry, M., & Zhang, J. (2020). *Prestress Loss Diagnostics in Pretensioned Concrete Structures with Corrosive Cracking*. Journal of Structural Engineering-asce, 146, 04020013. DOI: 10.1061/(ASCE)ST.1943-541X.0002554.

Dasar, A., Irmawaty, R., Hamada, H., Sagawa, Y., & Yamamoto, D. (2016). *Prestress Loss and Bending Capacity of Pre-cracked 40 Year-Old PC Beams Exposed to Marine Environment*. MATEC Web of Conferences 47,02008.DOI: 10.1051/ matecconf/20164702008.

Kottari, A.K., & Shing, P.B. (2014). *Estimation of Long-Term Prestress Losses in Post-Tensioned Girders*. Aci Structural Journal, 111, 1091-1100.

Lai L. (2016). *Research on how to modify data in PC girder bridge stress testing*, Chongqing Jiaotong University, Chongqing, China. (in Chinese)

Li, J., Miki, T., Yang, Q., & Mao, M. (2022). *Experimental Study on Prestressing Force of Corroded Prestressed Concrete Steel Strands*. Journal of Advanced Concrete Technology, 20, 550-563.

Ma Kunlin. (2009). *Mechanism and Evaluation Method of Salt Crystallization Attack on Concrete*, Central South University, China. (in Chinese)

Menga, A., Kanstad, T., Cantero, D., Bathen, L., Hornbostel, K., & Klausen, A.E. (2022). *Corrosion-induced damages and failures of posttensioned bridges: A literature review*. Structural Concrete, 24, 84 - 99.

Powers R.G., Sagues A.A. & Virmani Y.P. (2002). *Corrosion of post-tensioned tendons in Florida bridge*s. Public Works Research Institute, Technical Memorandum, (3843), 579, 2002.

Youakim, S.A., Ghali, A., Hida, S.E., & Karbhari, V.M. (2007). *Prediction of Long-Term Prestress Losses*. Pci Journal, 52, 116-130.